Novel Experiments and a Mechanistic Model for Macroinstabilities in Stirred Tanks

A. Paglianti, G. Montante, and F. Magelli
Department of Chemical, Mining and Environmental Engineering, University of Bologna –Viale Risorgimento 2, I-40136 Bologna, Italy

DOI 10.1002/aic.10634
Published online September 13, 2005 in Wiley InterScience (www.interscience.wiley.com).

In this work a new experimental technique and a simple model for the identification and the analysis of macro-instabilities (MIs) in stirred tanks are presented. A pressure transducer is proposed for detecting the MIs that can take place inside a stirred vessel; its main advantages are the non-intrusivity, cheapness, and simplicity of installation and operation. Moreover, it can be used for both laboratory and industrial scale stirred tanks. The experimental technique and the time series analysis method, based on Fast Fourier Transform (FFT), are shown to provide reliable information on the frequency of MIs, through the comparison of the present data with those, from literature, obtained in similar systems. Its applicability to solid-liquid systems is also assessed. Afterwards, the data collected in several conditions differing by geometric characteristics of the stirred tanks and by the physical properties of the systems are presented. Finally, a new simplified model, based on the theory of impinging jets,[1] is suggested for predicting the MI frequency. © 2005 American Institute of Chemical Engineers *AIChE J,* 52: 426–437, 2006
Keywords: macroinstabilities, mixing, pressure technique, various impeller types, fluid dynamics, impinging jets

Introduction

Stirred tank reactors are widely used in the process industry and, therefore, a large number of investigations have been carried out on the hydrodynamics of this equipment. So far, a significant amount of experimental and numerical work has allowed gaining a deep knowledge on the mean flow field and the turbulent characteristics in stirred vessels. Recently, many efforts have been devoted to the identification and the explanation of the so called macroinstability phenomenon that was observed to take place in stirred apparatuses in 1991 by Winardi and Nagase.[2]

Indeed, the MI phenomenon in stirred tanks has been the subject of numerous investigations and, consequently, several scientific works have been published on this topic in the last few years. A few techniques have been adopted for the experimental analyses: visual observation,[2-4] through which the MI presence is detectable only on a qualitative basis; laser doppler velocimetry[2,5-12] and particle image velocimetry (DPIV or PLIF),[13-18] which allow accurate measurement of the velocity time series and the MI frequency, but are both very costly and can be used only for transparent, laboratory-scale apparatuses; and finally, mechanical devices ("tornadometer,"[19] force measurement[20]), whose use is most likely limited to laboratory-scale stirred tanks.

Several authors have already pointed out the importance of taking the MI presence into account. According to Roussinova et al.,[21] one of the possible causes of errors of RANS-based CFD simulations could be due to the fact that the MI presence is disregarded; in fact, if the MIs are not properly accounted for, large errors can occur in the analysis of the velocity fluctuations, both in the impeller stream and in the upper part of the tank. Knowledge of MIs is important not only from the fluid dynamic point of view, but also for mechanical reasons[1,20]: if the MI frequency is equal to the characteristic frequency of the shaft, mechanical breakages can occur. More-

Correspondence concerning this article should be addressed to A. Paglianti at alessandro.paglianti@mail.ing.unibo.it.

over, when a fast chemical reaction takes place in a stirred tank reactor, the time scale of motion could be greater than the time scale of the reaction and, therefore, the performance of the stirred tank depends essentially on the MI behavior.[10] It has been shown that MIs have strong effects not only on the local heat transfer,[22] but also on the efficiency of mixing[23] and on the performance of biological reactors[24]. The influence of MIs on the mixing performances has been pointed out, among others, by Houcine et al.,[25] who showed that the intermittency can influence the macro- and meso-mixing, and by Guillard et al.,[17] who pointed out the importance of the instability of the coherent structures.

Nikiforaki et al.[10] sorted the possible instability phenomena in stirred vessels in three classes: the instabilities due to a change in the circulation pattern induced by a change in impeller clearance, the instabilities due to changes in flow patterns induced by a change in the Reynolds number, and, finally, the instabilities due to the unstable circulation pattern or to the presence of precessing vortices.

The first type of instabilities has been studied by Kresta and Wood,[26] who reported a change in flow pattern circulation for a pitched-blade turbine (PBT); by Montante et al.[27] and Galletti et al.,[28] who analyzed the change in flow pattern for a single Rushton turbine; and by Rutherford et al.,[29] who discussed the different flow patterns determined by two Rushton turbines placed at different relative distance.

The instabilities induced by a change in the Reynolds number have been studied, among others, by Hockey and Nouri[30] and Distelhoff et al.[31] for a vessel stirred by a PBT.

The last kind of instabilities is due to the unstable circulation pattern or the presence of precessing vortices.[32] The origin and the relation between these two kinds of instabilities is still a highly controversial question.[32-35] Kresta and Roussinova[32] suggested that the instabilities due to unstable circulation pattern probably depend on the pressure reflections on the jet and they can be sensitive to changes in impeller and vessel geometry; whereas, according to Galletti et al.,[8] the MIs due to precessional vortices play an important role at high impeller Reynolds number and their frequency is almost certainly linearly related to the impeller diameter. So far, because of the difference in the values of their characteristic frequencies, the two types of MIs have been considered as unrelated. Nevertheless, some analogies between the two phenomena can be identified, such as, for instance, their dependency on the ratio between the impeller diameter, D, and the tank diameter, T. Several authors[1,6,36,37] showed that the frequency of the instabilities stemming from unstable circulation patterns, f, changes linearly with the impeller rotational speed, N. Galletti et al.[8] and Hasal et al.[20] showed that both the instabilities due to unstable circulation patterns and those due to the precessing vortices change linearly with N. Moreover, after analyzing the two different types of MIs for Rushton turbines, Galletti et al.[8] suggested evaluating the dimensionless frequency, $f' = f/N$, with an equation of the form: $f' = a\,(D/T) + b$. The values of the constants, a and b, were found to be equal to 0.83 and -0.17, respectively, for the MIs due to unstable circulation patterns, whereas a was equal to 0.068 and b to 0.007 for the MIs due to precessing vortices. These simple relations, derived from experimental evidence, show that the two different kinds of MIs have some important analogies between each other.

In spite of the previous results, several questions can still be raised on the influence of the apparatus geometric characteristics on the MI frequency, which seems to be one of the major unclear points. Some of the questions have already been answered: for instance, the presence of a lid, for Rushton turbines and down-pumping pitched blade turbines, was shown not to affect the MI frequency,[10] and f' was found to be independent of the vertical position along the baffle.[20] On the other hand, some other aspects are still rather confused, as contradictory results have been obtained by different authors. For example, f' was found to be only slightly dependent on the impeller clearance for both a small[10] and a large scale vessel,[1] while a linear correlation between the frequency of MI and the off-bottom clearance was found in a vessel stirred by a Rushton turbine.[38]

One of the main inconsistencies concerns the dependency of the MI frequency on the impeller type. Montes et al.[6] suggested that with a four-bladed 45° PBT (D = T/3), the MI exhibits a characteristic dimensionless frequency, f', equal to 0.0575 for Re = 75,000, while f' was found to be equal to 0.09 for Re = 1140. Brůha et al.[37] investigated the effect of the flow regime for a vessel stirred with a six-bladed 45° PBT and identified the absence of MI phenomena in the laminar regime, the dependency of f' on the Reynolds number under the transitional regime, and a constant f' value in the fully turbulent regime. Myers et al.[13] obtained f' = 0.011-0.023 with a 4-bladed PBT (D = 0.35 T); Roussinova et al.[1] found f' = 0.186 for a large-scale 4-bladed 45° PBT (D = 0.5T) at various C/D ratios; Baudou et al.[12] found f' = 0.037 for a TT Mixel (D/T = 0.33); Roussinova and Kresta[7] found f' in the range 0.1-0.13 for an A310 impeller (D/T = 0.58); and Winardi and Nagase[2] identified unstable motion with f' = 0.02-0.03 with a marine propeller. It is worth observing that the results obtained by different authors reported above seem to suggest that f' is strongly dependent on the impeller type, but the spread in the f' values is significant even for geometrically similar impellers.

Therefore, one of the main goals of this study was to reconcile the large number of literature experimental data and suggest a simple model to evaluate the frequency of MIs due to unstable circulation patterns or the presence of precessing vortices, by changing impeller type and geometric characteristics of the tank and of the impeller. Moreover, in the following sections, the frequency of the MI will be shown to be measurable by using a simple pressure transducer instead of complex techniques, as those usually adopted in the aforementioned investigations. The set-up suggested in the present work could be used in industrial stirred tanks for evaluating the MI frequency by using widespread and cheap instrumentation.

Experimental Procedures

The experiments were performed in two cylindrical stirred tanks of different scales, the smaller of diameter, T, equal to 0.23 m and the larger of T equal to 0.49 m. In the following, the two tanks will be named T23 and T49, respectively. Both vessels were made of Perspex and were provided with a flat bottom and four vertical baffles having a width of 0.1T and attached to the wall. In almost all cases, the liquid level, H, was kept equal to T. In some experiments, the vessels were provided with a lid. The larger tank was agitated with two different impellers: either a 6-bladed 45° PBT or a 4-bladed 45° PBT, whose diameter, D, was equal to 0.160 m and 0.196 m, respectively. The smaller tank was agitated with five different impel-

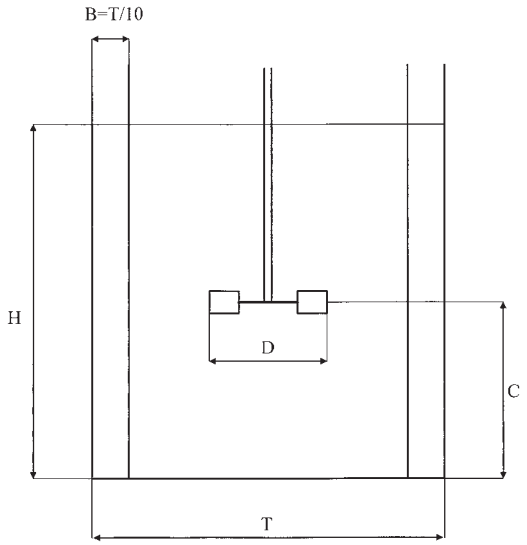

Figure 1. Vessels showing the main geometric parameters.

lers: a Lightnin A310 (D = 0.132 m), two Rushton turbines (D = 0.115 m and 0.078 m), a 6-bladed 45° PBT (D = 0.160 m), and a Lightnin A315 impeller (D = 0.178 m). For the T49 vessel, the impeller off-bottom clearance, C, was fixed at 0.33T for all the experiments, while for the smaller vessel the impeller's clearance was varied from 0.15T to 0.5T. As the liquid phase, tap water or a solution of water and polyvinylpyrrolidone (PVP) with a constant viscosity, μ, of 7.4 mPa·s and a density, ρ, of 1005 kg/m^3, were used. In all cases, the experiments were run at room temperature. Most of the experiments have been carried out in single-phase conditions, but some measurements have also been done in a solid-liquid system using, as the dispersed solid phase, glass particles of mean diameter, d_p, equal to 125 μm and density, ρ_s, equal to 2500 kg/m^3. Solid loads up to 40% by weight were tested. A rotational Reynolds number corresponding to fully turbulent conditions was kept for almost all the measurements. For the smaller tank, agitation was provided by a 70 W three-phase induction motor with rotational speed controlled by a manual device; for the larger tank, a 2.2 kW three-phase induction motor controlled by an inverter was used. In both cases, a digital tachometer was used to measure the impeller rotational speed. The geometric characteristics of the two stirred vessels are depicted in Figure 1.

The pressure time series were measured by a simple transducer based on a silica chip and a slim diaphragm of 2.54 mm^2 surface, which was able to reveal small pressure variations. The transducer was inserted in the reactors by side-wall ports placed midway between two consecutive baffles in the larger vessel, whereas in the smaller vessel it was placed 30 degrees up-stream of a baffle. For the measurements in the smaller vessel, the axial elevation of the port was fixed at 85 mm from the vessel bottom, while for the larger vessel several axial positions were considered, the lowest one being at 4 cm from the bottom. Therefore, the measurement point coincided with the small volume close to the vessel wall at the elevation and the tangential position of the specific port adopted for the connection between the vessel and the transducer.

The signal from the pressure transducer was amplified and the time traces were recorded and transferred to a personal computer by a data acquisition card controlled by a simple LabView® program. For each experimental run, a time history ranging from 15 to 60 minutes was recorded and a typical sampling frequency of 500 Hz was adopted. The influence of both the acquisition rate, which was changed from 100 up to 1000 Hz, and the sampling time was carefully checked in advance. The calibration line for the conversion of the measured voltage to pressure is shown in Figure 2, where a very good linear correlation between the signal and the pressure can be observed (the correlation coefficient of the calibration line was practically equal to 1). The spectral distribution of the pressures was obtained using an FFT method implemented in the MatLab® software. The typical frequency resolution of the spectral distribution was equal to 0.016 Hz. It is worth observing that with the pressure technique the time interval between the samples is uniform; thus, the use of standard spectral methods (such as FFT), which are based on equidistant times between samples, is possible. Therefore, interpolation techniques are not required to obtain evenly sampled time series from unevenly sampled data as, for example, in the case of LDA data; as a result, high frequency resolution is easily obtainable.

For selected conditions, the time evolution of an electrolytic tracer in the T49 tank was also measured by a conductivity method in solid-liquid systems. From the conductivity recordings, C_t, the dimensionless conductivity time series, C^*, were obtained with the following equation

$$C^* = \frac{C_t - C_{t=0}}{C_{t=\infty} - C_{t=0}}, \tag{1}$$

where $C_{t=0}$ is the initial conductivity value and $C_{t=\infty}$ is the value corresponding to complete homogenization conditions. For each measurement, the starting time (t = 0 s) corresponds to the tracer injection. Indeed, the data acquisition system was designed so that a trigger signal is recorded once the tracer starts entering into the tank. A sampling frequency equal to 400 Hz was selected. The conductivity probe position was fixed at 35 cm from the vessel bottom, while the tracer was injected at different elevations.

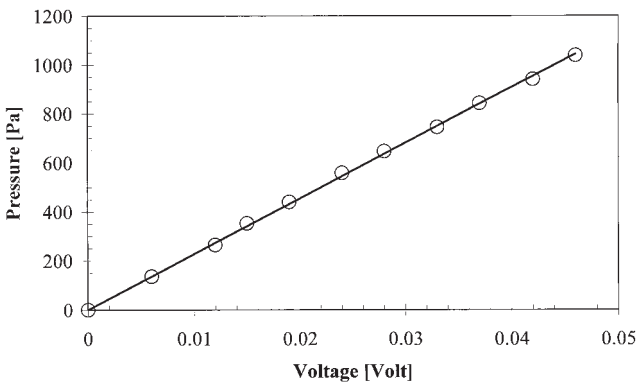

Figure 2. Calibration curve for the pressure transducer.

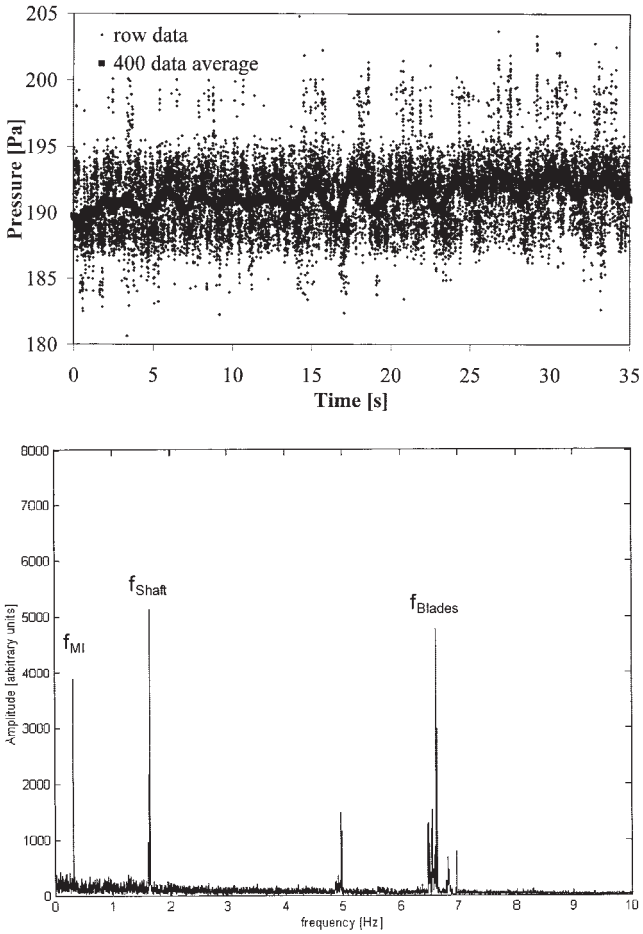

Figure 3. Data collected in the T23 vessel stirred with the A315 impeller in down-pumping mode. N = 100 rpm.

(a) Pressure time trace, symbols: raw data, line: averaged data; (b) frequency spectrum of the pressure signal.

Results and Discussion

Typical results and data validation

A characteristic pressure-time trace is shown in Figure 3a. In particular, the pressure signal was recorded for the smaller tank (T23) filled with the more viscous liquid and stirred by a Lightnin A315 impeller (down-pumping mode, located at C = T/2) at the speed, N, of 100 rpm. In the same Figure, overlapped with the raw time trace, the signal resulting from the mean of 400 data is shown, evaluated by means of a moving-window average technique. The complete recording consisted of about 2 million points acquired at a rate of 500 Hz, but in Figure 3a the time scale is limited to 35 s for a clearer representation. A large-scale cyclic variation of the signal can be identified, whose characteristic period is approximately equal to 3 s, corresponding to a frequency, f, equal to 0.33 Hz. The frequencies of the same signal can be observed in Figure 3b, where the frequency spectrum of the pressure recording is plotted. Pronounced peaks can be observed at frequencies corresponding to the shaft (1.67 Hz) and the blades passage (6.67 Hz), together with the characteristic frequency of 0.33 Hz; this last is approximately identifiable from the moving

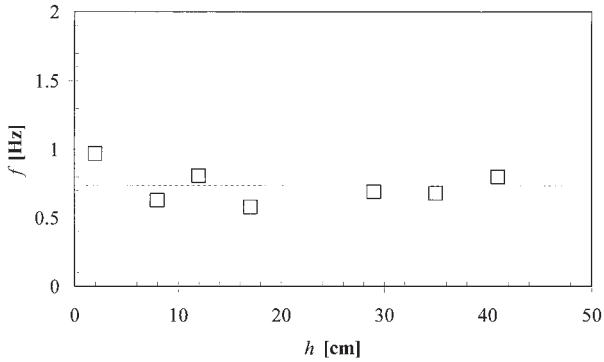

Figure 4. Data collected in the T49 vessel stirred with the 4-bladed PBT impeller in down-pumping mode. N = 571rpm. Effect of transducer vertical position on the MI frequency.

average data in Figure 3a and corresponds well to the long period instabilities, much longer than the blade passage frequency, already named macroinstabilities.

The dependency of the low frequency peaks on the particular measurement location was also checked for a single impeller speed (N = 571 rpm) in the T49 vessel. In Figure 4 the value of the macroinstabilities frequency obtained at different elevations from the vessel bottom is shown. As can be observed, the frequency of the macroinstabilities changes from about 0.6 to 0.7 for all the positions except for the lowest point where the frequency is about 0.9. Definitely, the frequency of the long period instabilities was very slightly modified with the location, while a distinct variation in peak amplitude in the frequency spectra relative to the various elevations was observed. The first step of the work consisted in evaluating the capability of the newly developed experimental technique to provide reliable data for the flow instability investigation. To this end, stirred tank configurations already adopted in other works have been considered, and the results have been compared with the available literature data. The details of the geometric configurations used to test the method and the corresponding literature conditions are shown in Table 1. In Figure 5, the comparison between the dimensionless frequencies, f', obtained in the present work and those reported in the literature, all relative to the conditions given in Table 1, are shown. In all cases, fully turbulent conditions and single-phase systems were considered. Good agreement between the two sets of data is noticeable; indeed, the error mean square is about 9%. It is important to stress that the f' values obtained with the Lightnin A310 impeller and with the PBT are relevant to MI associated to unstable circulation patterns,[6,7] whereas those identified with

Table 1. Geometric Details of the Stirred Vessel Configurations Adopted in this Work for the Evaluation of the Accuracy of the Technique and Details Relevant to the Cases Selected from the Literature

Present Data			Literature		
Impeller Type	*C*/*T*	*D*/*T*	Author	*C*/*T*	*D*/*T*
Lightnin A310	0.33	0.57	Roussinova & Kresta ([7])	0.39	0.58
Rushton Turbine	0.50	0.34	Galletti et al. ([8])	0.50	0.33
6-bladed PBT	0.33	0.33	Montes et al. ([6])	0.35	0.33

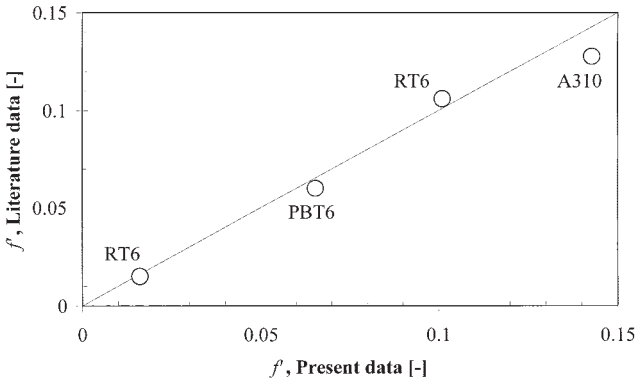

Figure 5. Comparison of dimensionless frequency of the macroinstability, f', in this work and from literature, relative to the geometric configurations reported in Table 1.

the RT are related both to the unstable circulation pattern and the presence of precessing vortices.[8] The good agreement of the results shown in Figure 5 allows concluding that, once a proper data acquisition frequency is selected and a time trace long enough is recorded, the MI frequency can be accurately evaluated by using simple pressure transducers as the measuring device.

Interpretation of present and literature data

Once the reliability of the devised method was assessed, the first question on the MI phenomenon that we tried to answer was: is the MI appearance due to pressure reflections on the jet, as suggested by Kresta and Roussinova,[32] or is it caused by different interactions?

In Figures 6a and b, the characteristic pressure frequency spectra obtained in the T23 vessel stirred at 150 rpm with the Lightnin A315 impeller, located midway between the vessel free surface and its bottom (C = 0.5T) and working in either down-pumping and up-pumping mode, respectively, are shown. In order to change the pumping mode, the impeller blade side was turned upside down and the shaft rotational speed was changed from clockwise (down-pumping mode) to anticlockwise (up-pumping mode). Two low frequency peaks, at 0.48 and 1.4 Hz, can be clearly identified when the impeller works in the down-pumping mode (Figure 6a), whereas no such peaks can be identified if the impeller works in the up-pumping mode, apart from those associated to the shaft and the blades passage frequencies, which are obviously identical for both the impellers rotational wise. It is worth observing that the major difference between the situations of Figure 6a and 6b is related to the direction of the main jet induced by the impeller: for the down-pumping mode it impinges against the bottom wall, while for the up-pumping mode it flows towards the free surface. In this last case, the jet impingement, JI, against the free surface does affect also the precessional vortices. The presence of the two low frequency peaks, most likely corresponding to the so-called MI and JI frequencies,[9] in the first case, and the absence of any predominant low frequency peak in the second one, suggest that the instabilities can be related to the pressure reflections of the jet against the wall (MI_J) or to a precessing vortex close to the shaft (MI_V).

In order to expand the theoretical interpretation to as many cases as possible, the low frequency instabilities data collected in this work have been analyzed together with those available from literature, relative to various geometric configurations and vessel scales, as well as to different flow regimes. So far, for almost every one of the investigated vessel geometric configurations, a linear correlation has been obtained between frequencies and impeller rotational speeds; but once the data collected from different systems are shown in the same plot, the scattering among them is significant. Some of the experimental data available in the literature, most of whose references are given in Table 2, as well as those obtained in the present work are shown in Figure 7, where the dimensionless frequency has been plotted against D/T, and a wide dispersion of data is evident. In Figure 8, the data collected with only two impeller types, i.e., A310 and PBT4, are shown (data reference in Table 3). It is worth noting that an almost linear trend of the data relative to the same impeller is apparent, the difference between the two being due to the different flow number of the

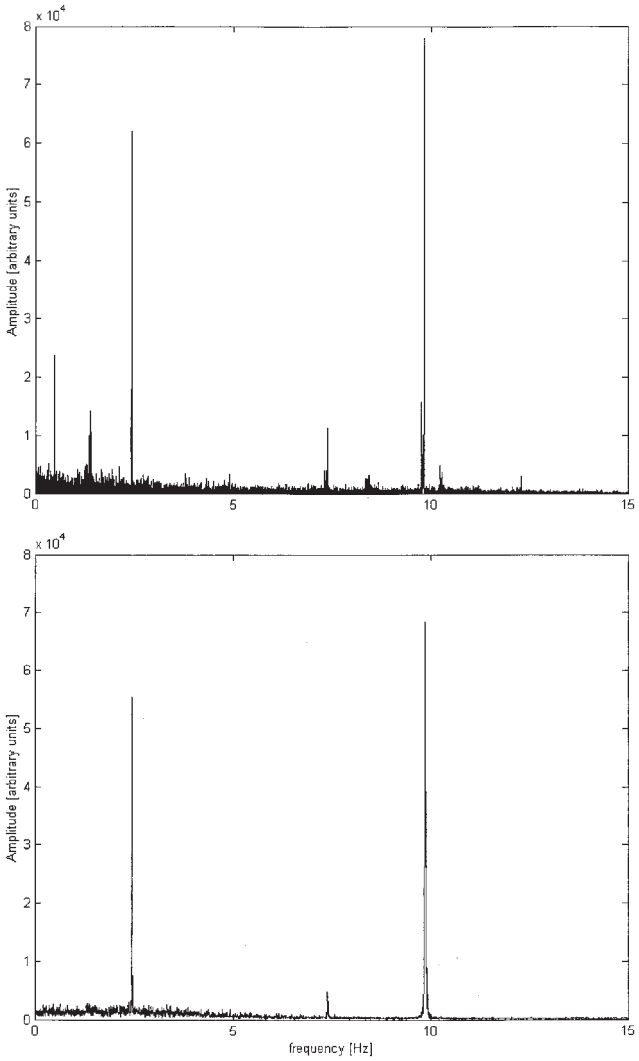

Figure 6. Frequency spectrum of the pressure time series collected in the T23 vessel stirred with the A315 impeller. N = 150 rpm.

(a, Top) down-pumping mode, (b, above) up-pumping mode.

Table 2. Geometric Details of the Stirred Vessel Configurations Adopted by Various Authors for the Study of the Macroinstabilities and Relevant Flow Numbers

Author	Impeller Type	D [m]	T [m]	F_Q
Baldi ([42])	RT	0.033	0.294	0.72
Baudou et al. ([12])	TTMixel	0.095	0.19	0.63
Brůha et al. ([19])	6-PBT	0.1	0.3	0.73
Fan et al. ([14])	RT4	0.14	0.28	0.62
Galletti et al. ([8])	RT	0.098-0.1941	0.294	0.72
	4-PBT	0.136	0.294	0.79
Galletti et al. ([9])	4-PBT	0.136	0.29	0.79
	RT	0.097	0.29	0.72
Guillard et al. ([18])	RT	0.1	0.3	0.72
Haam et al. ([22])	RT	0.129	0.387	0.72
Hasal et al. ([43])	6-PBT	0.1	0.3	0.73
Hasal et al. ([20])	RT	0.1	0.3	0.72
	4-PBT			0.79
	6-PBT			0.73
Jahoda et al. ([44])	6-PBT	0.097-0.145	0.29	0.73
Kilander & Rasmuson ([16])	A310	0.064	0.194	0.56
Kovács et al. ([45])	RT	0.267	0.8	0.72
Micheletti & Yianneskis ([11])	RT	0.027-0.098	0.081; 0.294	0.72
Montes et al. ([6])	6-PBT	0.1	0.3	0.73
Myers et al. ([13])	4-PBT	0.102	0.292	0.79
	HE3	0.114	0.292	0.41
Nikiforaki et al. ([10])	RT	0.098	0.294	0.72
Nikiforaki et al. ([46])	6-PBT 60 degree	0.098	0.294	0.99
Roussinova et al. ([21])	4-PBT	0.06-0.12	0.24	0.79
	A310	0.139		0.56
Roussinova et al. ([47])	4-PBT	0.12-0.61	0.24; 1.22	0.79
	A310	0.139-0.427	0.24; 1.22	0.56
Roussinova et al. ([1])	4-PBT	0.61	1.22	0.79
Roussinova et al. ([39])	4-PBT	0.08	0.24	0.79
Winardi & Nagase ([2])	Propeller	0.16	0.4	0.5
Present data	RT	0.078-0.115	0.232	0.72
	4-PBT	0.196	0.49	0.79
	6-PBT	0.16	0.232; 0.49	0.73
	A315	0.178	0.232	0.73
	A310	0.132	0.232	0.56

two impellers; therefore, the possibility to express the dependency of f' on impeller type or to any parameter related to the impeller is worth further investigation. Roussinova et al.[1] showed that the dimensionless frequency f', that is, the ratio between the MI frequency and the relevant impeller rotational speed, N, can be considered as the Strouhal number, St, for a stirred tank. Indeed, St, on which the impinging jet theory is usually centered, is defined as

$$St = \frac{f \cdot L_c}{V_c}, \tag{2}$$

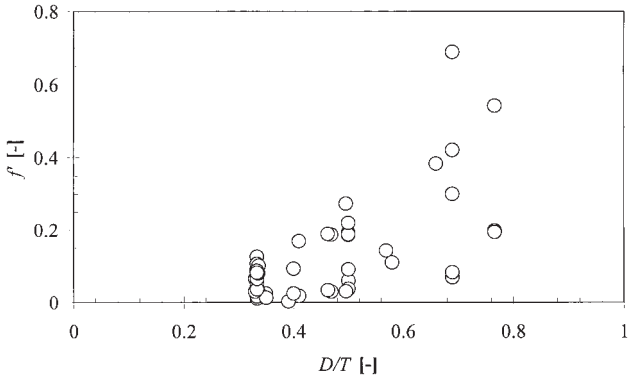

Figure 7. Effect of the D/T on the dimensionless frequency (cases of Table 2).

where L_c and V_c are the characteristic length and velocity scale, respectively, and f is the characteristic frequency.

In the present work, as a rough approach, we suggest replacing V_c with the mean velocity based on the impeller pumping capacity

$$V_c = \frac{F_Q \cdot N \cdot D^3}{A}, \tag{3}$$

where F_Q is the impeller flow number and A is the surface through which the impeller pumps the fluid out, which depends on the impeller type. For a radial impeller, A coincides with the lateral surface swept by the impeller blade tip and, therefore, the characteristic velocity can be evaluated as

$$V_c = \frac{F_Q \cdot N \cdot D^3}{\pi \cdot D \cdot H_b}, \tag{4}$$

where H_b is the blade height. For a standard Rushton turbine, H_b is equal to $0.2D$; thus, V_c becomes

$$V_c = c_{imp} \cdot F_Q \cdot N \cdot D, \tag{5}$$

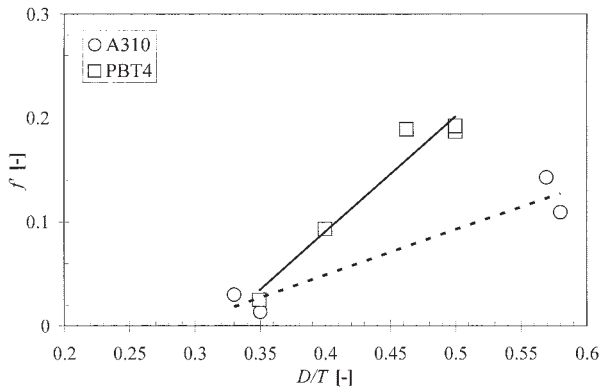

Figure 8. Effect of the D/T on the dimensionless frequency (cases of Table 3). Solid line: linear correlation of the PBT4 data; dotted line: linear correlation of the A310 data.

Table 3. Details of Selected Stirred Vessel Configurations Adopted for the Study of the Macroinstabilities Grouped by Impeller Type

Impeller Type	Author	D/T	F_Q
A310	Kilander & Rasmuson ([16])	0.33	0.56
	Roussinova et al. ([47])	0.35; 0.58	0.56
	Present data	0.57	0.56
4-bladed PBT	Galletti et al. ([8])	0.46	0.79
	Myers et al. ([13])	0.35	0.79
	Roussinova et al. ([21])	0.5	0.79
	Roussinova et al. ([47])	0.5	0.79
	Present data	0.4	0.79

where c_{imp} is a constant equal to $5/\pi$. For axial flow impellers, A coincides with the impeller bottom surface, i.e., the area of a circle of diameter equal to D; the characteristic velocity can be evaluated with Eq. 5, but the constant c_{imp} is equal to $4/\pi$.

As for the length scale, L_c, one of the characteristic dimensions of either the tank or the impeller can be adopted, i.e., T or H for the tank and D, C, or the distance from the side walls for the impeller. It is worth recalling that the impeller off-bottom clearance has been found to have negligible effect on the MI frequency.[10,39]

In this work the effect of the impeller distance from the side wall has also been investigated. In Figure 9 the frequency of the instabilities against the impeller rotational speed is plotted for three different sets of data, collected in the T23 vessel equipped with a Rushton turbine (D = T/3, C = T/2) in symmetric and eccentric configurations. In this last case, the shaft was set midway between two neighboring baffles at 55 mm from the wall. The transducer was fixed to the side wall closer to the turbine (position A) or at the opposite side (position B). As can be observed, for each condition, two different characteristic low frequencies were often identified, but, in any case, the position of the turbine seems to have negligible effects on the frequencies. The reason for the different low frequencies will be discussed later on. As the geometric parameters relevant to the impeller position seem not to be dramatically important for the MI frequency, we choose to refer to the tank geometry and to adopt the tank diameter T as the characteristic length. With these assumptions, the Strouhal number becomes

$$St = \frac{f \cdot T}{c_{imp} \cdot F_Q \cdot N \cdot D}. \tag{6}$$

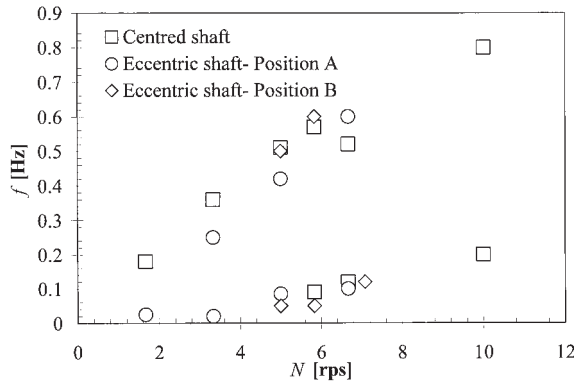

Figure 9. Effect of the shaft position on the f vs. N data.

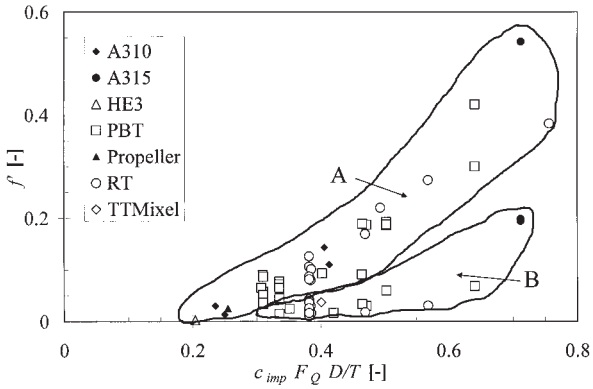

Figure 10. Effect of the impeller type on the dimensionless MI frequency.

Therefore, the dimensionless frequency f' is a function of the flow number F_Q, the impeller diameter D, and the tank diameter T

$$f' \propto \frac{c_{imp} \cdot F_Q \cdot D}{T}. \tag{7}$$

It is worth noting that the assumption of L_c equal to T implies that the present model agrees with the empirical equations suggested by Galletti et al.,[8] who found that the dimensionless MI frequency, f', is linearly dependent on the D/T ratio.

In Figure 10 the experimental data obtained in the present work and some experimental data available in literature are shown according to Eq. 7, that is, the dimensionless frequency, f', is plotted against $(c_{imp} \cdot F_Q \cdot D)/T$.

As can be observed, the experimental data can be divided into two sets, each grouped with a line. On the basis of previous analyses, the first group of data, labeled with A, can be considered coincident with the MI_J. They can be fitted very closely with a line whose equation is

$$f' = 0.852 \cdot \frac{c_{imp} \cdot F_Q \cdot D}{T} - 0.215. \tag{8}$$

The accuracy of the correlation can be evaluated with a correlation coefficient, which is equal to 0.884 (Figure 11). The second group of data, labeled B in Figure 10, contains the MI_V and is plotted in Figure 12. In this case, a linear correlation is not adequate at all.

Apparently, MI_J and MI_V macroinstabilities cannot be described with the same approach. For the former, which are originated from the impeller jet, it is reasonable to consider a mean velocity based on the impeller pumping capacity; while for the latter, which are most likely associated with the precessional vortices taking place close to the liquid surface, probably it is more appropriate to consider a different characteristic velocity. For this purpose, a mean liquid velocity in the upper part of the tank can be considered, defined as

$$V_c = \frac{Q}{(\pi \cdot T^2)/4}, \tag{9}$$

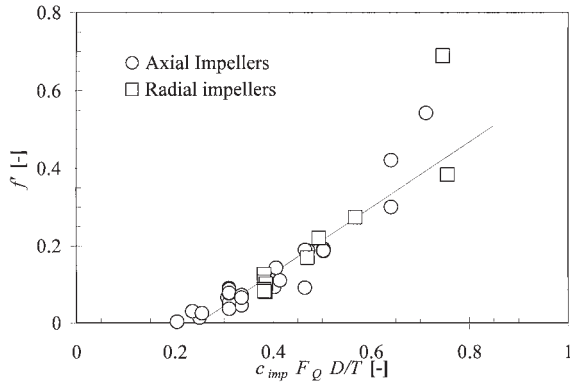

Figure 11. Group A data. Effect of the impeller type on the dimensionless MI_J frequency; f' vs. c_{imp} F_Q (D/T).

where Q is the volumetric flow-rate flowing in the upper part of the total tank.

If a single loop is established, it is possible to assume that

$$Q = F_Q \cdot N \cdot D^3. \tag{10}$$

whereas, if a symmetric double loop takes place, half of the total flow-rate flows in the upper part of the vessel and half in the lower part, hence:

$$Q = \frac{1}{2} F_Q \cdot N \cdot D^3. \tag{11}$$

Consequently, the characteristic velocity can be evaluated as:

$$V_c = F_{imp} \cdot F_Q \cdot \frac{N \cdot D^3}{T^2}, \tag{12}$$

where F_{imp} is a constant equal to $4/\pi$ and $2/\pi$ for the single loop and symmetric double-loop regime, respectively.

The introduction of Eq. 12 in the Strouhal number definition, together with the hypothesis of $L_c = T$ also for MI_V, leads to a modified equation for the dimensionless frequency

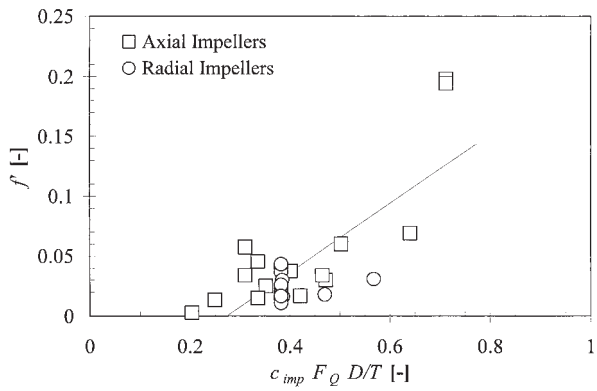

Figure 12. Group B data. Effect of the impeller type on the dimensionless MI_V frequency; f' vs. c_{imp} F_Q (D/T).

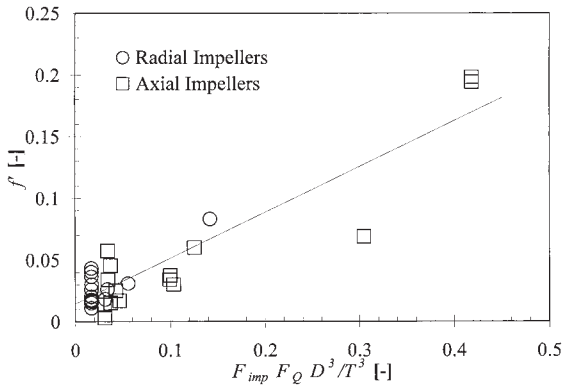

Figure 13. Group B data. Effect of the impeller type on the dimensionless MI_V frequency; f' vs. F_{imp} F_Q $(D/T)^3$.

$$f' \propto \frac{F_{imp} \cdot F_Q \cdot D^3}{T^3}. \tag{13}$$

Eq. 13 coincides with that derived for a vessel stirred with a 45° 6-bladed PBT by Brůha et al.[37] (see their Eq. 6).

Apparently, in the case of macroinstabilities originated from precessional vortices, MI_V, the dimensionless frequency, f', is not any more linearly dependent on the D/T ratio, as for the case of MI_J, but it depends on the same ratio to a cubic exponent. In order to verify if such a hypothesis can lead to a better data correlation, the same dimensionless frequencies, f', of Figure 12 are replotted against $(D/T)^3$ in Figure 13. As can be observed, the linear equation

$$f' = 0.372 \cdot \frac{F_{imp} \cdot F_Q \cdot D^3}{T^3} + 0.014, \tag{14}$$

provides an acceptable fit (with a correlation coefficient equal to 0.824). The larger scatter of the experimental data with respect to the MI_J case, especially in the low f' range, could be due to the experimental uncertainties connected with the acquisition time length adopted by various authors. In fact, it is to be observed that the lower the unstable event frequency is, the longer the acquisition time has to be to obtain a reliable spectrum in the low frequency region.

Also, it is important to point out that the present simplified approach agrees also with the results of the numerical simulations performed by Hartmann et al.[40] In fact, from the theoretical approach suggested by Hartmann et al.,[40] based on LES analysis, a dimensionless frequency, MI_v, of 0.0228-0.0255 arises for a Rushton turbine stirred tank, whereas by using the present simplified approach a frequency of 0.021 is estimated.

This simplified approach could explain why, for Rushton turbines, a small decrease in the dimensionless frequency occurs once the clearance is increased, as shown in Figure 14. Probably, this behavior is to be related to the flow field above the turbine. Indeed, if the impeller off-bottom clearance is equal to 0.15T, a single loop regime establishes, whereas if the clearance is equal to 0.5T the turbine produces a double loop pattern. The difference in the liquid flow rate and, consequently, in the velocity produced in the upper part of the vessel

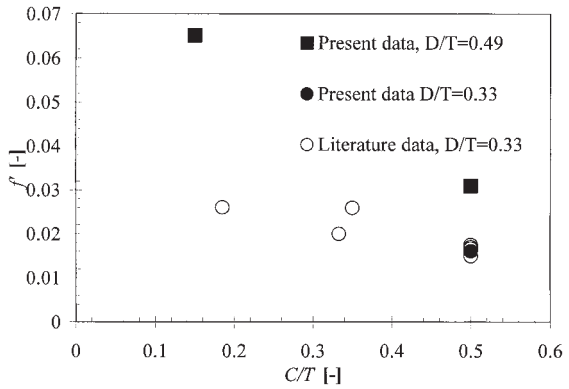

Figure 14. Effect of the impeller clearance on the MI_v frequency for RT.

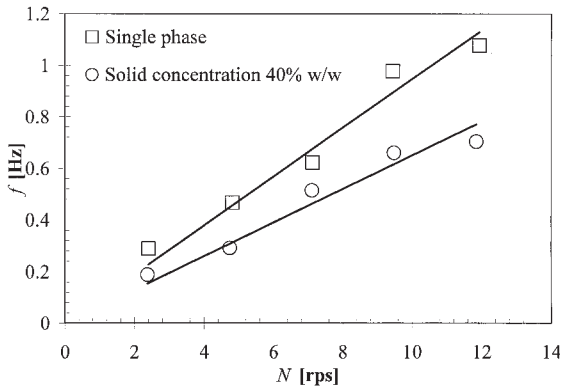

Figure 15. Effect of solid concentration on MI frequency for the T49 vessel equipped with a 4-bladed PBT.

in the two cases is, probably, responsible for the different values of the dimensionless frequency shown in Figure 14 (the details of the geometric configurations are shown in Table 4).

Solid-Liquid systems and mixing time measurements

The experimental technique described above has also been adopted to perform measurements in solid-liquid systems, with the main aim of verifying its applicability to multiphase flows. The results obtained in the T49 vessel are shown in Figure 15, where a variation of the instability frequency with the impeller rotational speed is apparent for a single and a two phase system (i.e., water and a suspension of glass particles in water). Generally, the present data qualitatively agree with those obtained by Jahoda et al.,[4] who showed that the MI frequency is affected by the addition of a dispersed solid phase to the stirred liquid; in particular, the frequency of the instabilities was found to decrease with increasing the solid concentration. A wider range of physical properties of the two phases and geometric characteristics of the stirred tanks should be investigated for a deeper insight into the effect of the solid concentration on the MI phenomena. Nevertheless, the present data allow assessing that the pressure technique can be confidently used not only for single phase systems, but also for dense two-phase systems for which optical techniques, such as PIV and LDA, are inadequate.

Finally, the influence of MIs on the mixing performances of stirred tanks has been investigated through experiments of tracer homogenization carried out by a conductivity method in the T49 vessel. The experiments consisted of the injection of a small amount of an aqueous salt solution inside the stirred tank and recording of the conductivity time trace. Each experiment was carried out at least three times in order to assess the repeatability of the results. A dense solid-liquid system was used instead of a single phase in order to visualize the vortices. Indeed, the solid particles allow identifying clearly the location of the slowly moving vortex, and the tracer injection was performed inside or outside the vortex with good accuracy. The reliability of the method was verified by comparing the results obtained in three different runs carried out under each condition. For the experiments in the solid-liquid system, the data are affected by both the presence of the solid particles and of the tracer, because the probe measures the local conductance of the whole medium. Therefore, for a proper analysis of the homogenization curves and an accurate evaluation of the mixing time, the bias of the solid concentration fluctuations has to be eliminated. For this reason, the contribution of the solid particle passage to the recorded signal has been filtered out. A clear indication of the contribution of the solid passage in the control volume to the conductivity signal can be obtained from the analysis of the data relative to the time interval between the acquisition start and the tracer injection. Different from the case of single phase flow, the signal experiences significant fluctuations. The extent of such fluctuations can be appreciated in Figure 16a, where the time trace measured before tracer injection, at an impeller speed equal to 570 rpm, is shown (time equal to zero corresponds to the tracer injection). This trace was analyzed with an FFT technique, and the resulting frequency spectrum is shown in Figure 16b; as can be observed, the solid fluctuations are characterized by well defined low frequencies in the range of 0.5-5.0 Hz. The contribution of such fluctuations was filtered out when analyzing the concentration time series, as they are clearly due to the solid passage inside the measurement volume rather than to the tracer.

Jahoda et al.[4] have shown that for solid-liquid systems stirred with a PBT, macro-vortices are formed at the interface defined by an ascending stream of suspension along the vessel wall and the descending stream coming from the baffle trailing edge. Starting from this information, which was confirmed by visual observation of our T49 vessel filled with the solid-liquid dispersion, the tracer injections were performed in the macro-vortices regions as well as in those regions where macro-vortices are absent. For this reason, the probe position was

Table 4. Details of Some of the Stirred Vessel Configurations Adopted for the Study of the Macroinstabilities with Rushton Turbines

Author	*D/T*	*C/T*
Baldi ([42])	0.33	0.50
Galletti et al. ([8])	0.33	0.50
Galletti et al. ([9])	0.33	0.185
Hasal et al. ([20])	0.33	0.35-0.5
Nikiforaki et al. ([10])	0.33	0.50
Nikiforaki et al. ([46])	0.33	0.33-0.5
Present data	0.34	0.5
	0.5	0.15-0.5

fixed at 35 cm from the vessel bottom, while the injection point was changed along the vessel axis at the same distance from the vessel wall. In Figure 17 the homogenization curves relative to the tracer injected either inside a macro-vortex at h = 29 cm or far from it at h = 8 cm, a region where macro-vortexes are absent, are shown. As can be observed in Figure 17, when the injection takes place inside a macro-vortex (h = 29 cm), the mixing time is definitely longer. In fact, for the injection at 8 cm from the bottom, after 5.8 s from the injection the salt concentration is bounded in the range ± 15% of the final value; whereas if the injection is performed inside a macro-vortex, even at times greater than 17 s the salt concentration exhibits oscillations bigger than ± 15%. In the past, an improvement in mixing performance was observed[41] in some low velocity regions. In this work it has been shown that a worsening in the mixing performance of the reactor can be produced if the injection point of a reactant is located in the zone where macro-vortices are forming.

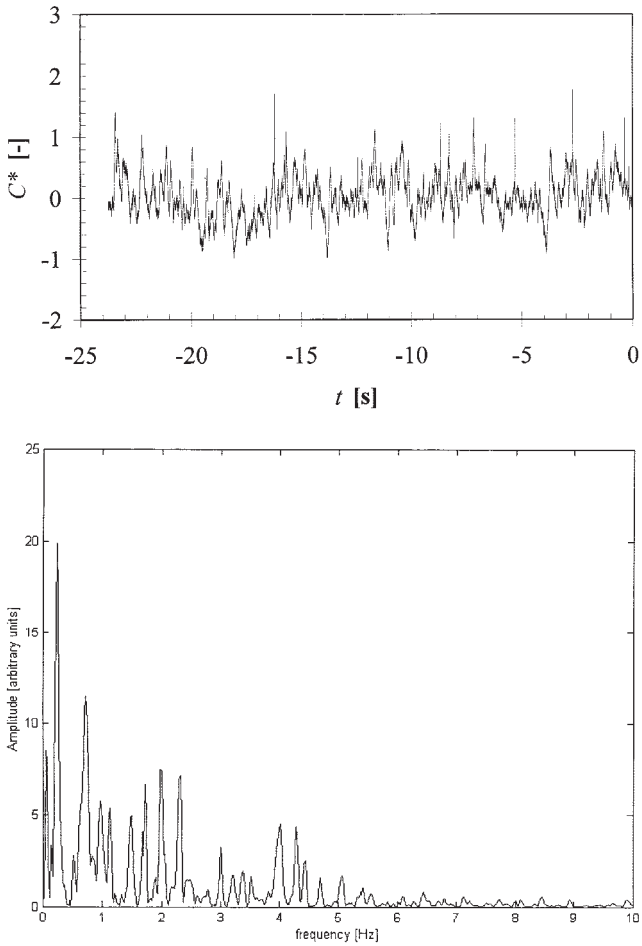

Figure 16. Dimensionless conductivity signal in the T49 vessel stirred with the 4-bladed PBT in down-pumping mode. N = 570 rpm.

(a, Top) fluctuations due to the solids before the tracer injection, (b, above) frequency spectrum of the solid concentration signal.

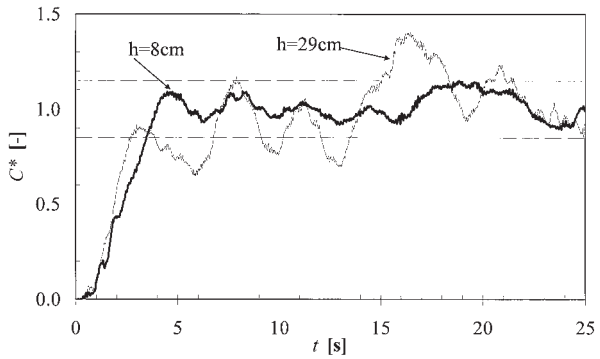

Figure 17. Homogenization curves in the solid-liquid system in the T49 vessel stirred with the 4-bladed PBT (down-pumping mode); N = 570 rpm; effect of the MI on the mixing time.

Conclusions

In this work, a simple technique to detect macroinstabilities in stirred tanks and to identify their frequency has been presented. The method is based on the acquisition of pressure time traces and on their analysis with Fast Fourier Transform. As opposed to other techniques, based on optical methods, such as LDA, PIV, or visual observations, the present method can be easily used in industrial stirred tanks and multiphase systems; therefore, useful information on the fluid dynamics can be obtained and unexpected apparatus performances can be avoided. Besides the above-mentioned advantages for application in industrial processes, the present method can be used also in laboratory scale equipment to study systems where optical methods are inadequate (e.g., stirred tanks with high solid contents).

Furthermore, a simple model, based on impinging jet theory, has been proposed that reconciles the large amount of data available in the literature. Two equations are derived that permit predicting with acceptable accuracy both the frequency of the macroinstabilities due to impinging jets (MI_J) and those due to precessional vortices (MI_V).

Finally, the influence of the MIs on the mixing performance has been investigated through a few homogenization experiments based on a conductivity method. The MI phenomena have been confirmed to considerably affect the mixing operations.

Acknowledgments

This work was financially supported by the University of Bologna and the Italian Ministry of University and Education (FIRB 2001 project and PRIN 2003). The collaboration of Messrs. Francisco Navarro Moreno and Daniele Fajner in carrying out the experimental program is gratefully acknowledged.

Notation

A = impeller swept area [L^2]
B = baffle width [L]
C = off-bottom impeller clearance [L]
C^* = dimensionless conductivity [–]
c_{imp} = dimensionless geometric constant (Eq. 5) [–]
D = impeller diameter [L]
d_p = solid particle diameter [L]
f = MI frequency [T^{-1}]

f' = f/N, dimensionless MI frequency [–]
F_Q = Q^*/ND^3, impeller flow number [–]
F_{imp} = dimensionless constant (Eq. 12) [–]
h = axial position [L]
H = vessel height [L]
H_b = blade height [L]
L_c = characteristic length [L]
N = rotational speed [T^{-1}]
Q = volumetric flow-rate in the upper part [L^3T^{-1}]
Q^* = impeller pumping capacity [L^3T^{-1}]
Re = $\rho ND^2/\mu$, Reynolds number [–]
St = $f L_c/V_c$, Strouhal number [–]
T = vessel diameter [L]
V_c = characteristic velocity [L^1T^{-1}]
μ = dynamic liquid viscosity [$MT^{-1}L^{-1}$]
ρ = liquid density [ML^{-3}]
ρ_s = solid density [ML^{-3}]

Literature Cited

1. Roussinova V, Kresta SM, Weetman R. Low frequency macroinstabilities in a stirred tank: scale-up and prediction based on large eddy simulations. *Chemical Engineering Science.* 2003;58:2297-2311.
2. Winardi S, Nagase Y. Unstable phenomenon of flow in a mixing vessel with a marine propeller. *Journal of Chemical Engineering of Japan.* 1991;24:243-249.
3. Chapple D, Kresta S. The effect of geometry on the stability of flow patterns in stirred tanks. *Chemical Engineering Science.* 1994;49: 3651-3660.
4. Jahoda M, Machoň V, Vlach L, Fořt I. Macro-instabilities of a suspension in an axially agitated mixing tank. *Acta Polytechnica.* 2002; 42:3-7.
5. Montes JL, Boisson HC, Fořt I, Jahoda M. Local study of velocity field macro-instabilities in mechanically agitated fluids in a mixing vessel. Proc of 12th CHISA, Praha, Lecture D3.3, 1996.
6. Montes JL, Boisson HC, Fořt I, Jahoda M. Velocity field macro-instabilities in an axially agitated mixing vessel. *Chemical Engineering Journal.* 1997;67:139-145.
7. Roussinova V, Kresta SM. Analysis of macro-instabilities (MI) of flow field in a stirred tank agitated with axial impellers. Proc. 10th European Conference on Mixing, Delft, The Netherlands, 2000:361-368.
8. Galletti C, Paglianti A, Lee KC, Yianneskis M. Reynolds number and impeller diameter effects on instabilities in stirred vessels. *AIChE Journal.* 2004;50:2050-2063.
9. Galletti C, Paglianti A, Yianneskis M. Observations on the significance of instabilities, turbulence and intermittent motions on fluid mixing processes in stirred reactors. *Chemical Engineering Science.* 2005;60:2317-2331.
10. Nikiforaki L, Montante G, Lee KC, Yianneskis M. On the origin, frequency and magnitude of macro-instabilities of the flows in stirred vessels. *Chemical Engineering Science.* 2003;58:2937-2949.
11. Micheletti M, Yianneskis M. Precessional flow macro-instabilities in stirred vessels: study of variations in two locations through conditional phase-averaging and cross-correlation approaches. Proceedings 11th Int. Symposium on Application of Laser Techniques to Fluid Mechanics, Lisbon, 2004.
12. Baudou C, Xuereb C, Costes J, Bertrand J. Laser doppler measurements of turbulent parameters in different multiple-propeller systems. *Chemical Engineering & Technology.* 2000;23:257-266.
13. Myers KJ, Ward RW, Bakker A. A digital particle image velocimetry investigation of flow field instabilities of axial-flow impellers. *Journal of Fluids Engineering.* 1997;119:623-632.
14. Fan J, Wang Y, Rao Q, Fei W. A study on intermittency phenomena in the impeller stream via digital particle image velocimetry (DPIV). *Chemical Engineering Journal.* 2004;102:25-33.
15. Fan J, Wang Y, Rao Q, Fei W. Spatio-temporal analysis of macro-instability in a stirred vessel via digital particle image velocimetry (DPIV). *Chemical Engineering Science*. 2004;59:1863-1873.
16. Kilander J, Rasmuson A. Hydrodynamics in a stirred square tank investigated using a 3-D PIV LES decomposition approach and LDA measurements. *Chemical Engineering & Technology.* 2004;27:270-274.
17. Guillard F, Trägårdh C, Fuchs L. A study on the instability of coherent mixing structures in a continuously stirred tank. *Chemical Engineering Science.* 2000;55:5657-5670.
18. Guillard F, Trägårdh C, Fuchs L. A study of turbulent mixing in a turbine-agitated tank using fluorescence technique. *Experiments in Fluids.* 2000;28:225-235.
19. Brůha O, Fořt I, Smolka P. Flow transition phenomenon in an axially agitated system. *Proceedings of the 8th European Conference on Mixing. (IChemE Symposium series).* 1994;136:121-128.
20. Hasal P, Fořt I, Kratěna J. Force effects of the macro-instability of flow pattern on radial baffles in a stirred vessel with pitched-blade and Rushton turbine impellers. *Chemical Engineering Research and Design.* 2004;82:1268-1281.
21. Roussinova V, Grgic B, Kresta SM. Study of macro-instabilities in stirred tanks using a velocity decomposition technique. *Chemical Engineering Research and Design.* 2000;78:1040-1052.
22. Haam S, Brodkey RS, Fasano JB. Local heat transfer in a mixing vessel using heat flux sensors. *Industrial & Engineering Chemistry Research.* 1992;1:1381-1391.
23. Muzzio FJ, Meneveau C, Swanson PD, Ottino JM. Scaling and multifractal properties of mixing in chaotic flow. *Physic of Fluids. A.* 1992;4:1439-1456.
24. Namdev PK, Yegneswaran PK, Thompson BG, Gray MR. Experimental simulation of large scale bioreactors environments using a Monte Carlo method. *Canadian Journal of Chemical Engineering.* 1991;69: 513-519.
25. Houcine I, Plasari E, David R, Villermaux J. Feedstream jet intermittency phenomenon in a continuous stirred tank reactor. *Chemical Engineering Journal.* 1999;72:19-29.
26. Kresta SM, Wood PE. The mean flow pattern produced by a 45° pitched blade turbine: changes in the circulation pattern due to off bottom clearance. *Canadian Journal of Chemical Engineering.* 1993; 71:42-53.
27. Montante G, Lee KC, Brucato A, Yianneskis M. Double- to single-loop flow pattern transition in stirred vessels. *Canadian Journal of Chemical Engineering.* 1999;77:649-659.
28. Galletti C, Brunazzi E, Yianneskis M, Paglianti A. Spectral and wavelet analysis of the flow pattern transition with impeller clearance variations in a stirred vessel. *Chemical Engineering Science.* 2003;58: 3859-3875.
29. Rutherford K, Mahmoudi SMS, Lee KC, Yianneskis M. Hydrodynamics characteristics of dual Rushton impeller stirred vessels. *AIChE Journal.* 1996;41:332-346.
30. Hockey R, Nouri JM. Turbulent flow in a baffled vessel stirred by a 60° pitched blade impeller. *Chemical Engineering Science.* 1996;19: 4405-4421.
31. Distelhoff MFW, Laker J, Marquis AJ, Nouri JM. The application of strain gauge technique to the measurement of the power characteristics of five impellers. *Experiments in Fluids.* 1995;20:56-58.
32. Kresta SM, Roussinova VT. Comments to "On the origin, frequency and magnitude of macro-instabilities of the flows in stirred vessels." *Chemical Engineering Science.* 2004;59:951-953.
33. Yianneskis M. Reply to the Comments by Kresta to "On the origin, frequency and magnitude of macro-instabilities of the flows in stirred vessels." *Chemical Engineering Science.* 2004;59:955-956.
34. Yianneskis M. Reply to the Comments by Fořt to "On the variation of precessional flow instabilities with operational parameters in stirred vessels." *Chemical Engineering Journal.* 2004;104:99.
35. Fořt I. Comments to "On the variation of precessional flow instabilities with operational parameters in stirred vessels." *Chemical Engineering Journal.* 2004;104:97.
36. Brůha O, Fořt I, Smolka P. Phenomenon of turbulent macro-instabilities in agitated systems. *Collection of Czechoslovak Chemical Communications.* 1995;60:85-94.
37. Brůha O, Fořt I, Smolka P, Jahoda M. Experimental study of turbulent macro-instabilities in an agitated system with axial high-speed impeller and radial baffles. *Collection of Czechoslovak Chemical Communications.* 1996;61:856-867.
38. Matsuda N, Tada Y, Hiraoka S, Qian S, Takeda H. The effect of off-bottom clearance on macro instabilities in stirred vessel. *Journal of Chemical Engineering of Japan.* 2004;37:1215-1233.
39. Roussinova VT, Kresta SM, Weetman R. Resonant geometries for circulation pattern macroinstabilities in a stirred tank. *AIChE Journal.* 2004;50:2986-3005.
40. Hartmann H, Derksen JJ, van den Akker HEA. Macroinstability un-

covered in a Rushton turbine stirred tank by means of LES. *AIChE Journal.* 2004;50:2383-2393.
41. Larsson G, Törnkvist M, Ståhl Wernersson E, Trägårdh C, Noorman H, Enfors SO. Substrate gradients in bioreactors: origin and consequences. *Bioprocess Engineering.* 1996;14:281-289.
42. Baldi S. Energy dissipation measurements in stirred vessels with particle image velocimetry. Ph.D. Thesis, King's College London, London, UK, 2004.
43. Hasal P, Montes JL, Boisson HC, Fořt I. Macro-instabilities of velocity field in stirred vessel: detection and analysis. *Chemical Engineering Science.* 2000;55:391-401.
44. Jahoda M, Parůžek K, Machoň V, Fořt I. Interaction of flow macro-instabilities and free liquid surface in an agitated vessel. Proc. 11th European Conference on Mixing, Bamberg, Germany, 2003:605-612.
45. Kovács T, Trägårdh C, Fuchs L. Fourier spectrum to recover deterministic and stochastic behavior in stirred tanks. *AIChE Journal.* 2001;47:2167-2176.
46. Nikiforaki L, Yu J, Baldi S, Genenger B, Lee KC, Durst F, Yianneskis M. On the variation of precessional flow instabilities with operational parameters in stirred vessels. *Chemical Engineering Journal.* 2004; 102:217-231.
47. Roussinova V, Weetman R, Kresta SM. Large eddy simulations of macroinstabilities in a stirred tank with experimental validation at two scales. North American Mixing Forum Conf., Pocono Manor, PA, 2001.

Manuscript received December 9, 2004, and revision received June 15, 2005.